CHARACTERIZATION OF A SUPERSONIC WIND TUNNEL FOR THE STUDY OF SUPERSONIC INLET FLOW CONTROL

A THESIS

Presented in Partial Fulfillment of the requirements for Graduation with Distinction in the Department of Mechanical Engineering at The Ohio State University

By

Aaron W. Porter

The Ohio State University

2012

Abstract

The geometry and the nature of supersonic flow in supersonic mixed compression inlets generate internal shock wave/boundary layer interactions (SWBLIs). Shock waves generated by the inlet cause internal boundary layer disruptions that lead to inlet inefficiencies and possible boundary layer separation. Boundary layer separation is undesirable because it reduces mass flow to the engine and can lead to choking of the inlet or unstart. Current flow control methods are effective in reducing the separation, but are yet to significantly increase the inlet efficiency. Researchers at the Gas Dynamics and Turbulence Laboratory (GDTL) have proposed a new control technique using localized arc-filament plasma actuators (LAFPAs). The LAFPAs are to be tested in a supersonic blow down wind tunnel with a compression ramp shock generator. The characterization of the baseline flow of this facility is vital to researching control of the interaction. Several qualitative and quantitative flow diagnostics were used to characterize this Mach 2.3 flow. The interaction generated in this tunnel was shown to be a separated SWBLI comparable with those studied in literature. It was also found to exhibit the expected low frequency unsteady behavior.

Acknowledgments

I would first like to thank Professor Samimy for providing the opportunity to join his research team. I am grateful for his constant encouragement to bring him any questions and for his help in my understanding of one dimensional gas dynamics. For my colleagues, Nathan Webb and Chris Clifford, I am thankful for their guidance and patience as they explained shock wave/boundary layer interactions and experimental techniques. I appreciate the time they took to ensure that I understood the information completely as well as their continued support as I finish my schooling. I am also thankful for the rest of the members of the Gas Dynamics and Turbulence Laboratory who provided intellectual conversations throughout my time in the laboratory. Finally, I would like to thank my family and friends who have supported and encouraged me through all of my schooling and research.

I would also like to thank the Air Force Research Laboratory (Mr. Jon Tinapple and Dr. Jonathan Poggie) and the Air Force Office of Scientific Research (Dr. John Schmisseur) for their support of this research.

Table of Contents

List of Figures

List of Tables

Chapter 1: Introduction

Mixed compression engine inlets are designed to improve the efficiency of supersonic flight vehicles. The inlet achieves better pressure recovery in compressing the air and reducing it to subsonic speeds through the use of multiple oblique shock waves, which are weaker than normal shock waves. Oblique shock waves are formed at the inlet cowl and interact with the boundary layer on the inlet surfaces, called a shock wave/boundary layer interaction (SWBLI). This supersonic flow phenomenon is commonly found in the aerospace industry on aircraft wings and in mixed compression inlets.

In mixed compression inlets, strong interactions can cause the boundary layer to separate. Flow separation occurs when the fluid momentum in the boundary layer is insufficient to overcome adverse pressure gradients imposed by the shock waves. Flow separation decreases the effective cross sectional area of the inlet and can cause choking and unstart. Unstart occurs when the upstream mass flow is greater than the downstream mass flow resulting in the shock system moving upstream and eventually out of the inlet. This causes the engine to stall and results in rapid deceleration of the aircraft.

The adverse consequences of SWBLI induced flow separation in supersonic inlets have motivated research to reduce and control the interaction. Boundary layer bleed is a method to reduce flow separation by the removal of the low momentum fluid through scoops and holes placed upstream of SWBLI locations, thereby increasing the health of the boundary layer (Syberg and Koncsek 1976). However, the bleed system incurs losses and adds complexity to the engine. The bleeding reduces the performance of the inlet as it causes a reduction in the mass flow rate. To counteract this, larger inlets are used, incurring losses through weight and

drag. Also, the complex ducting of this system results in difficult design and manufacture of these engines as well as increased costs.

Boundary layer bleed is effective but not efficient, thus motivating the development of alternative flow control methods to reduce separation. Flow control can be divided into two categories: passive and active. Passive flow control uses geometric modifications to energize the boundary layer or to alter the shock structure. Anderson et al.(2006) used micro-ramps and micro-vanes and Babinsky et al. (2009) also used micro-ramps to create streamwise vortices to mix the free stream and boundary layer flow. Three dimensional bumps have also been used to modify the shock structure and increase total pressure recovery (Ogawa and Babinsky 2008).

Active flow control either uses the natural instabilities in the flow to amplify small localized energy inputs for manipulation of the flow phenomena of adds momentum to the flow. Kalra et al. (2011) used low current surface discharges forced by a moderate strength magnetic field to try to control SWBLIs. Leonov et al. (2008) have attempted to use surface-localized discharges to change the structure and parameters of the flow field. Researchers at the Gas Dynamics and Turbulence Laboratory (GDTL) are also trying to actively control the flow in the SWBLI using localized arc filament plasma actuators (LAFPAs). LAFPAs have previously been used for instability manipulation for jet noise mitigation and mixing enhancement. (Samimy et al., 2007a ; Samimy et al., 2007b; Samimy et al.2010).

Chapter 2: Background

2.1 Shock Wave/Boundary Layer Interactions

Oblique shock waves are formed when the inlet forces the flow to turn on itself, thereby generating a shock. In an internal flow, these waves will impinge on a surface and reflect, developing a shock system that terminates in a normal shock. In particular these shocks interact with the turbulent boundary layer on the internal surfaces of the inlet, potentially causing the boundary layer to separate. In strong interactions, the fluid momentum in the boundary layer is not able to overcome the adverse pressure gradient across the shock wave causing flow reversal and separation. The separation bubble alters the reflected shock location pushing it upstream of the separation. An illustration of this interaction is shown in Figure 1.

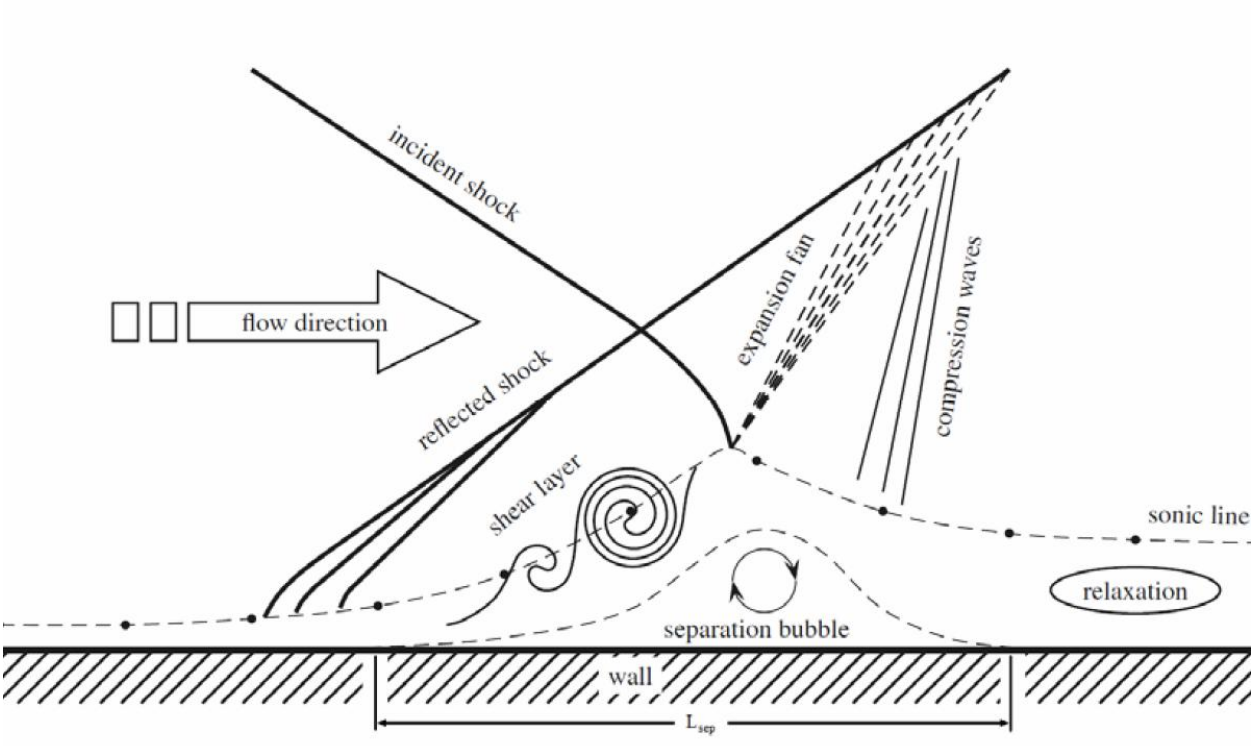

Figure 1: SWBLI (Touber and Sandham 2009)

The SWBLI has been studied for over fifty years but there are still aspects that are not well understood (Dolling 2001). One of the topics of ongoing research is the interaction unsteadiness when the flow is separated. The unsteadiness is associated with the reflected shock and the frequency is two orders of magnitude less than that of the turbulence in the incoming boundary layer. Dupont et al. (2006) have studied the unsteadiness and have shown that it scales with the interaction length. Touber and Sandham (2009) have also verified this finding through computational fluid dynamics. These groups have both concluded that the weighted power spectral density of the unsteadiness of the shock foot has a peak centered about a Strouhal number of 0.03. They have also found another unsteadiness with a peak at St=0.5 associated with the reattachment of the separation. Figure 2 shows the weighted power spectral density of the interaction near the shock foot. The Strouhal number discussed above has been defined by Dupont et al. (2006) to scale on the interaction length.

$$St = \frac{f * L_{int}}{U_{\infty}}$$

f = frequency (Hz)

L_{int} = length of the interaction (m)

U_{∞} = free stream velocity (m/s)

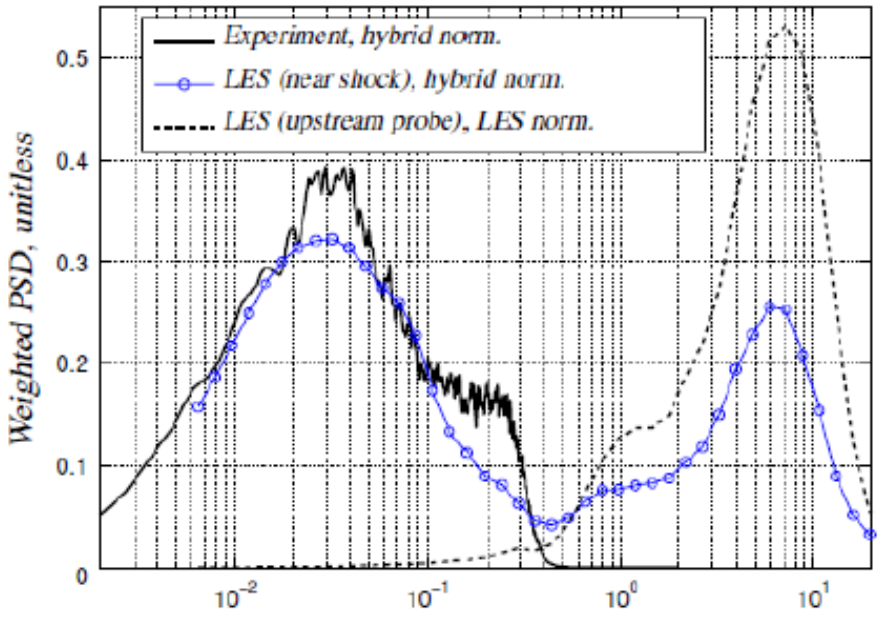

Figure 2: Weighted Power Spectral Density vs. Strouhal Number of a SWBLI (Touber and Sandham 2009)

There are two theories on the cause of the unsteadiness. One position is that the separation bubble experiences a "breathing motion" as it empties and refills itself, thereby forcing the reflected shock to oscillate (Piponniau et al. 2009). The other position is that streamwise-elongated structures ("superstructures") in the upstream boundary layer travel downstream and generate the low frequency unsteadiness. The exact mechanism is still being researched but this unsteadiness is of great interest from a flow control perspective.

2.2 SWBLI Control Methods

The boundary layer separation induced by SWBLIs disrupts the flow making decreasing or eliminating these effects a focus for the flow control community. Boundary layer bleed has been the primary method to decrease this separation. It involves removing the low momentum fluid upstream of the SWBLI. This method requires larger inlets to account for the mass flow that is lost through bleeding. This increases weight and drag, resulting in decreased overall

efficiency. In order to increase inlet efficiency, other methods are being researched. Some passive flow control methods have proven effective. Anderson et al. (2006) used micro-ramps and micro-vanes to energize the near-wall flow. This generated longitudinal vorticity which mixed the free stream fluid with the low momentum boundary layer resulting in an increase in momentum near the wall. Babinsky et al. (2009) have also used micro-ramps to prevent separation resulting in smaller spans of separation divided by cells of attached flow. Negative effects of passive flow control are that the modifications are inflexible; therefore, at off-design conditions the benefit is greatly reduced or removed and inherent drag is still present.

Active flow control is advantageous because it is dynamic and can be turned on and off potentially providing more control and saving energy simultaneously. Knowledge of the interaction is required to efficiently implement active flow control because the goal is to allow the naturally present phenomena to amplify the actuation. However, controllable mechanisms in the interaction are not well understood so active flow control is more difficult to implement. Kalra et al (2011) use an arc discharge with a magnetic force to try to accelerate the flow. Also, Leonov et al. (2008) try to modify the shock structure using surface discharges. LAFPAs are another flow control device that use high voltage to create a plasma filament between two electrodes in order to add controlling perturbations to the fluid (Caraballo et al. 2009).

2.3 Localized Arc Filament Plasma Actuators

Localized arc filament plasma actuators have been developed at The Ohio State University. They are high bandwidth and high amplitude actuators for high-speed and high Reynolds number jet control (Samimy et al. 2004). They are comprised of two tungsten electrodes and operate from a 7.4 kV voltage supply. An electric arc forms between the electrodes ionizing the air. This breakdown causes rapid localized heating which induces

thermal and pressure perturbations into the flow. The LAFPAs can be pulsed at very high frequencies providing frequency control of these perturbations. Figure 3 shows an image of eight LAFPAs in operation located in the floor of the supersonic wind tunnel.

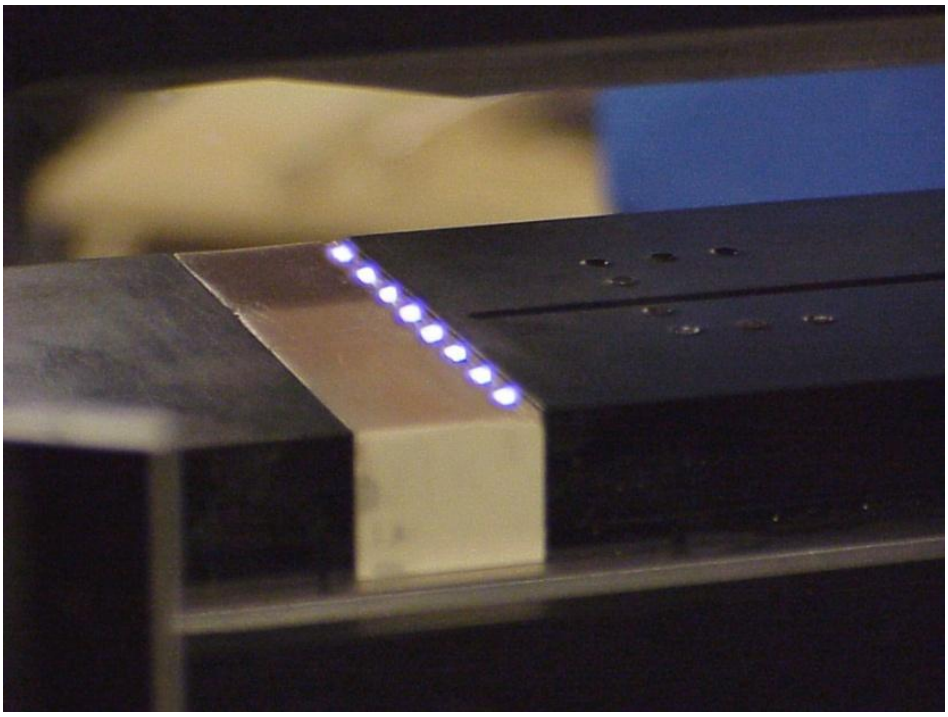

Figure 3: LAFPAs Being Operated in the Supersonic Wind Tunnel

The LAFPAs have proven effective in jet noise mitigation and mixing enhancement (Samimy et al., 2007a; Samimy et al., 2007b; Samimy et al.2010). The control authority of the LAFPAs leveraged the frequency control of the perturbations to manipulate the natural instabilities in the jet flow. This control authority motivated the use of LAFPAs for flow control of SWBLIs with their low frequency unsteadiness. The LAFPAs could add energy perturbations to the interaction and manipulate the natural instabilities of the interaction to mitigate or delay separation.

Chapter 3: Objective

Prior forcing of the LAFPAs in Mach 1.9 flow showed an effect on the separation, but the exact nature of the effect was unknown (Caraballo et al. 2009; Webb 2010). This facility was a small blow down facility with an incident shock generated by a 10^o compression ramp. For further investigation of the LAFPA control authority, a new facility was designed to improve the measurement constraints of the smaller facility. One constraint of this facility was the expansion wave's impingement on the interaction harming the data collected in this region. In turn, the increase in height of the new design would cause the expansion waves to impinge on the boundary layer further downstream, away from the interaction. The facility expansion also provides an opportunity for using different types of shock generators.

A new tunnel was designed and built increasing the height dimension from 1.5 in. to 2.87 in. A Variable Angle Wedge (VAW) was the shock generator for this new design providing flexibility. This wedge was placed in the flow removing the primary shock unsteadiness associated with compression ramp. It also provided an easy way to change wedge angle and height altering the shock strength and impingement location, respectively. This facility was characterized and the LAFPAs were tested; however, LAFPA effectiveness was no longer observed and data repeatability became an issue. Therefore, it was decided to design a 10^o compression ramp in an attempt to reproduce the interaction from the smaller tunnel.

The flow using this new shock generator must be characterized. The characterization helps to learn more about the SWBLI and possible mechanisms which might provide an opportunity for flow control. It also allows us to clearly assess the effects of control and the differences between the forced flow and the baseline. The flow will be measured through

qualitative and quantitative methods to establish the baseline and to characterize the flow of the SWBLI.

Chapter 4: Experimental Design and Methods

4.1 Tunnel Design

The variable compression ramp facility was a continuous blow-down type wind tunnel that exhausted to ambient air. The test section had a cross section of 3 in. width and 2.87 in. height and was preceded by a convergent divergent nozzle and a stagnation chamber. The nozzle accelerated the air to a measured Mach number of 2.3 and static temperature of roughly 140 K. The test section was observed through two windows on the side walls. These windows were formed of optical grade fused quartz; nominally 3 in. by 10 in. by .75 in. thick. They were removable, providing access into the test section. There was also a window in the ceiling that provided access for a laser sheet when performing streamwise-vertical oriented PIV. Figure 4 provides an image of the variable compression ramp facility.

Figure 4: Variable Compression Ramp Facility (Flow from Left to Right)

The primary shock was generated by the 10^{o} compression ramp mounted on the ceiling. The ramp spanned the width of the tunnel. It was fastened to the ceiling and can be moved to three streamwise locations to alter the impingement location of the primary shock. The test

section floor was designed carefully because of its effect on the placement of actuators and pressure transducers in relation to the separation. The floor was removable and was made of Delrin as shown Figure 5. There was a hole in the tunnel floor that was located off center for the placement of the actuator block. The actuator block housed the electrodes which were also placed at an off center location. These two eccentric placements allowed the LAFPAs to have four locations by flipping the actuator block or the floor.

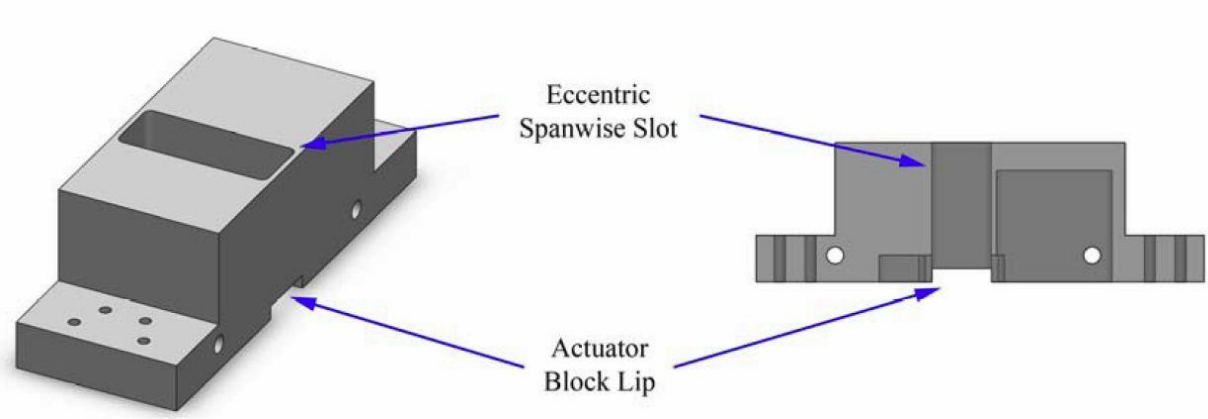

Figure 5: Delrin Test Section Floor (Clifford 2010)

The actuator block was a two piece design with boron nitride mounted on top of Delrin as shown in Figure 6. Boron nitride was chosen to house the LAFPAs because of its resistance to heat. There were eight LAFPAs evenly spaced in the actuator block. The electrodes of the LAFPAs were spaced 3 mm apart and the adjacent electrodes of two actuators were spaced 5 mm apart to prevent them from arcing to one another. They were also set in a groove to prevent the LAFPA arc from being blown downstream during tunnel operation. Other test section floors had been developed for other methods of measurement. For example, a blank floor was used for surface oil flow visualization, and there were floors made specifically for static and dynamic

pressure measurements. The tunnel floor had been designed for easy removal to assist in the swapping of these floors.

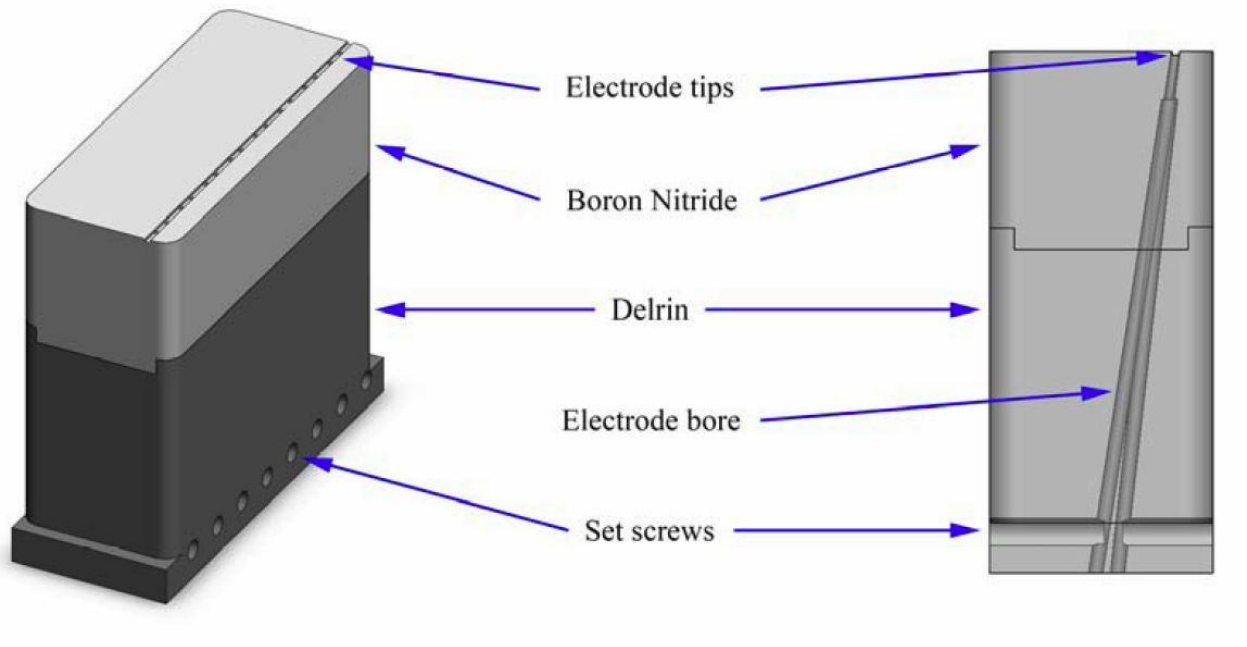

Figure 6: LAFPA Actuator Block (Clifford 2010)

4.2 Schlieren Imaging

Schlieren imaging is a nonintrusive qualitative flow measurement method that measures the density variations in a fluid. The density of the flow changes as it interacts with any disturbance, and the different densities result in different refractivity of light in connection to the Gladstone-Dale relation. Therefore, as the light passes through the facility, the light is refracted at different angles because of the density variation.

This technique uses a light source and optics to pass a collimated beam of light through the test section. A knife edge is placed at the focal point of the beam and it blocks any light

refracted in its direction. The result is light and dark regions corresponding to positive and negative gradients normal to the knife edge. The Schlieren setup is shown in Figure 7.

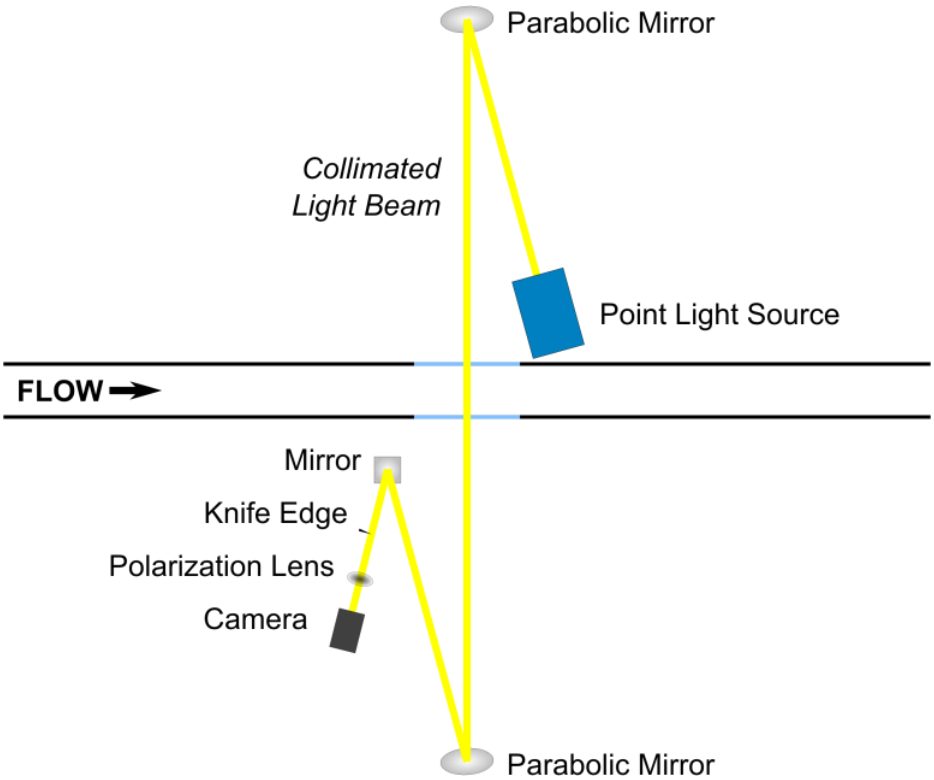

Figure 7: Optical Configuration for Schlieren Imaging

An LED light source with a single LED produced a steady beam for the time averaged data collection. The two parabolic mirrors were used for collimating the light and reflecting it through the test section. The camera used to capture the images was a Sony XCD-SX910 camera with a Nikon 55 mm lens, and the data was collected using NI LabVIEW 8 with NI-IMAQ camera control.

This technique measured density variations in the fluid which was advantageous for identifying shock waves. Many flow properties are nearly discontinuous across shock waves,

including the fluid density. Therefore, the sharp density variation signified shock waves and showed their location clearly. Schlieren imaging was a method to effectively observe the shock system and assisted in the identification of extraneous shocks.

This was a qualitative flow tool but it was very useful for measuring different parameters that are important for analyzing data. It was used to find the interaction length which was used as a normalization parameter. To find this length, the incident shock and reflected shock were extrapolated to the floor and the distance was measured between them. It was also used to find the shock impingement and actuator location.

Schlieren imaging inherently averaged in the spanwise direction because the light traveled through the entire width of the test section. The three dimensionality of the separation, discussed in 5.3, along with the spanwise averaging removed schlieren's ability to quantify LAFPA forcing effectiveness. However, it did provide a simple, easy diagnostic for parameter sweeps. Schlieren imaging can take time averaged images of the flow or instantaneous images using a flash light source with a trigger. For the scope of the baseline characterization, only time averaged images were needed.

4.3 Surface Oil Flow Visualization

Surface oil flow visualization was a qualitative technique used to examine the separation region, including its spanwise variation. This method observed the movement due to shear forces of a viscous mixture spread on the floor, providing a visual image of the separation effects. A mixture consisting of SAE 85W-140 gear oil and Titanium white oil pigment was combined to achieve the necessary viscosity. Oleic acid was also added as an anti-coagulant. It was then spread thinly on the Delrin floor in the area of the interaction.

For this experimental method, the flow was started quickly. During startup and while the tunnel was on, pictures were taken manually at approximately a 1 Hz rate with a Nikon D40 camera mounted a tripod. These pictures were later deskewed using computer software. After the surface oil finished spreading, the flow was shut down immediately to "save" the separation effects. Then, pictures were manually taken from a top down view of the resulting oil formation. The final position of the surface oil showed the extent of the separation, the impingement location, and the effects of the side wall separation.

4.4 Particle Image Velocimetry

Particle Image Velocimetry (PIV) measurements provided a quantitative view of the flow field. This measurement system used a laser beam produced by a Spectra Physics PIV 400 Nd:YAG laser, frequency doubled to a wavelength of 532 nm. The beam was converted into a sheet using a convex cylindrical lens and a spherical lens made the sheet thinner. This laser sheet was reflected from a mirror through the tunnel ceiling and into the test section. The schematic of this measurement setup is shown in Figure 8 below.

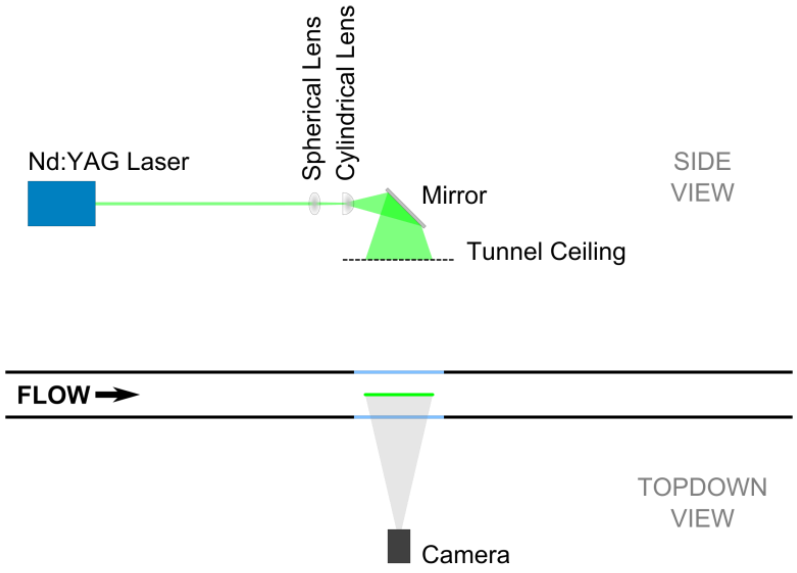

Figure 8: Optical Configuration for PIV

The laser sheet illuminated olive oil seed particles in the flow. The particles were injected into the upstream end of the stagnation chamber using a TSI 6 Jet atomizer. The turbulence reducing screens in the stagnation chamber aid in the even distribution of the particles throughout the flow. The particles were then captured using a LaVision Imager Pro CCD camera which took two images of the flow approximately 1.2 μs apart. The exact delay between images was captured through an oscilloscope for accurate velocity measurements. The two images were compared and LaVision DaVis 7.2 was used to track particles in the flow. The software uses the distance traveled and the time delay along with complex calculations and correlations to produce two dimensional velocity vector fields. For the characterization of the tunnel, approximately 500 vector fields were averaged to obtain a time averaged baseline flow field.

4.5 Unsteady Pressure Measurements

Unsteady pressure measurements on the tunnel floor were used to characterize the unsteadiness of the interaction. The experimental setup shown in Figure 9 used a Delrin floor that is made specifically for the dynamic pressure measurements. The locations for the pressure transducers were across a range of streamwise locations, from upstream to downstream of the interaction. The Kulite pressure transducers (model XTL-140-25A) have a frequency response up to 50 kHz which corresponds to St = 2.47 for our interaction. This ensures that the transducers were capable of measuring the low frequency unsteadiness of the interaction at St = 0.03 and St = 0.5. These pressure measurements can be used to verify that the SWBLI did have the low frequency unsteadiness associated with it that is known for these interactions.

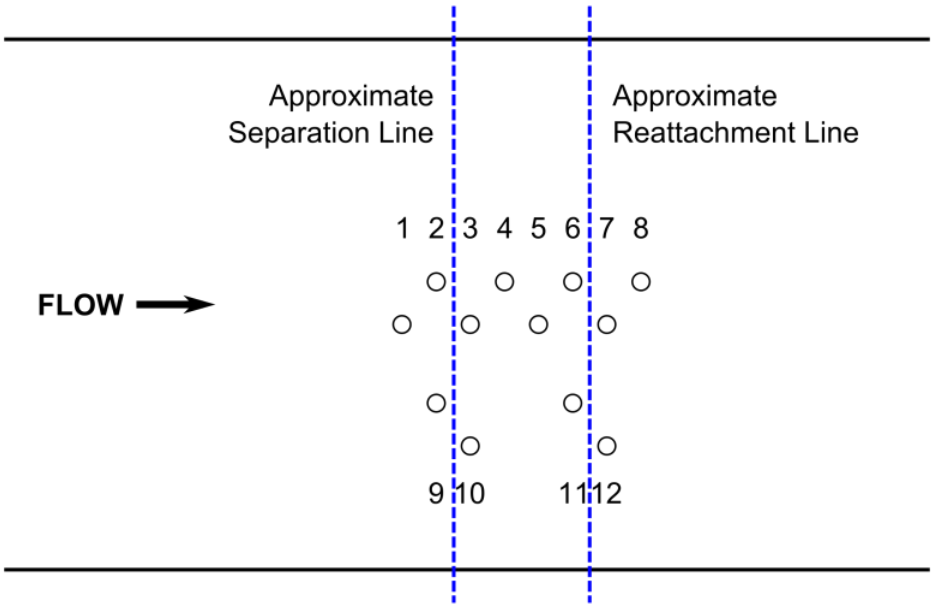

Figure 9: Kulite Pressure Transducer Arrangement for Unsteady Pressure Measurements

Chapter 5: Results and Discussion

5.1 Introduction

The new facility was designed with a 10^{o} compression ramp to generate the incident shock wave and form the SWBLI on the tunnel floor. The facility must be characterized to confirm that it was generating the expected interaction and to gain an understanding of the baseline flow before examining the control authority of the LAFPAs. There were numerous components of the flow to investigate including the primary shock, impingement point, extraneous shocks, expansion fans, separation, and interaction unsteadiness. Qualitative and quantitative experimental methods were used to verify the tunnel as an accurate SWBLI model.

5.2 Schlieren Imaging

After the compression ramp was placed into the test section ceiling, the tunnel was measured using Schlieren imaging. Schlieren imaging provided a view of the density gradients in the flow allowing shocks and their locations to be observed. The initial compression ramp design had a sharp tip at its lowest peak as shown in Figure 10. This figure also provided the expected shock location and arrangement for the flow. The actual flow arrangement is shown from Schlieren imaging in Figure 11 when the tunnel was operated.

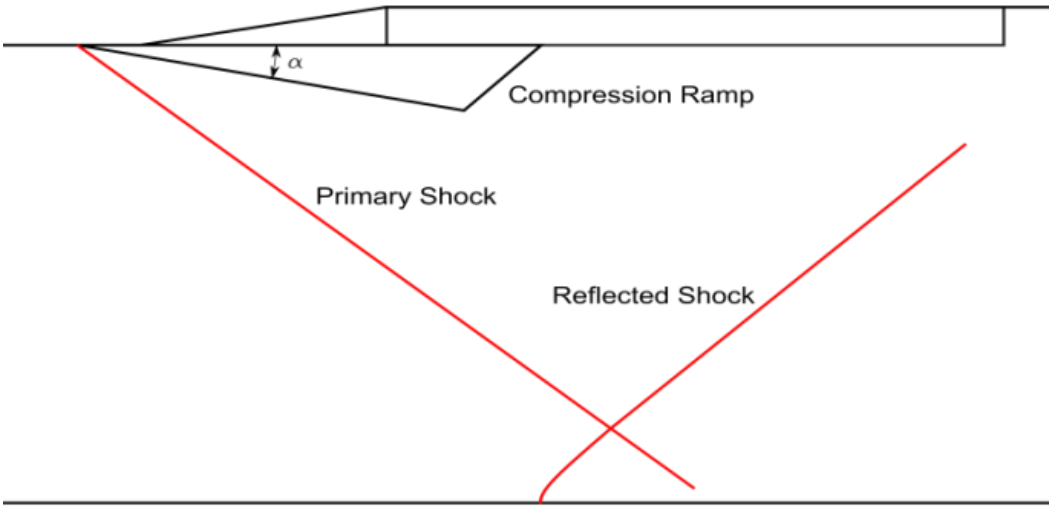

Figure 10: Expected Shock System from Theoretical Calculations

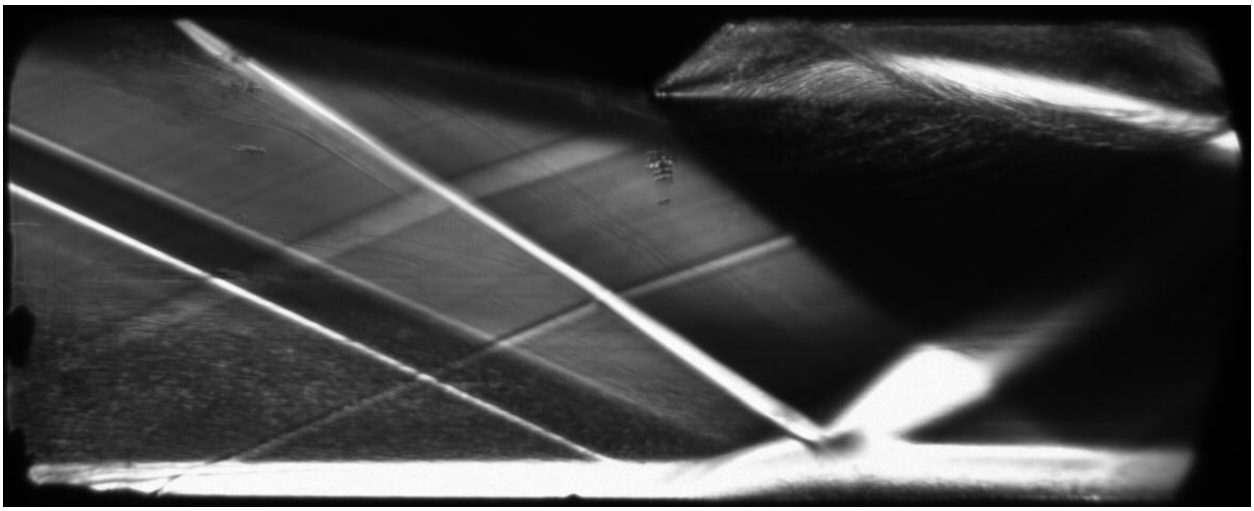

Figure 11: Schlieren Image with Sharp Tipped Compression Ramp

Figure 11 provided an image of the shock system of the Mach 2.3 air flow in the tunnel and the shocks were similar to Figure 10. The primary shock is the white line that begins at the foot of the compression ramp and it propagated to the test section floor. The increased boundary

layer height was due to the low momentum flow's response to the imposed adverse pressure gradient. The presence of separation was later confirmed using surface oil flow visualization. The reflected shock cannot be seen clearly as it is a black line, but it began at the beginning of the separation as expected. The horizontal knife edge used for these images resulted in the primary shock and reflected shock being represented by opposite intensities. This knife edge orientation did provide a clear view of the boundary layer allowing it to be observed.

Some extraneous shocks can be seen in the flow before the primary shock. These waves were caused by any imperfection on the tunnel surface or any obstruction. These were disregarded because they were weak and did not cause a noticeable effect on either the boundary layer or other shocks/expansions.

The expansion fan is the black triangle beginning at the trailing edge of the compression ramp. This expansion fan did not impinge on the tunnel floor until downstream of the reattachment line of the interaction which was one of the reasons for expanding the original facility. A white expansion fan can also be seen stemming from the interaction, but this fan is not important to the SWBLI studied.

However, the peak of the compression ramp was noted as a possible future problem. The peak protruded down from the ceiling a considerable amount which decreased the cross sectional area. From calculations, this cross sectional area was very near to the critical area. This was undesirable because the tunnel throat needs to be the smallest effective area for the proper operation of the tunnel. In this design, if the separation on the floor were to increase in strength, the effective area between the peak and the floor would decrease and could unstart the tunnel. To eliminate the possibility of this problem, the peak of the ramp was machined to be

flatter as shown in Figure 12. This provided more cross sectional area and a safe tolerance to prevent unstart.

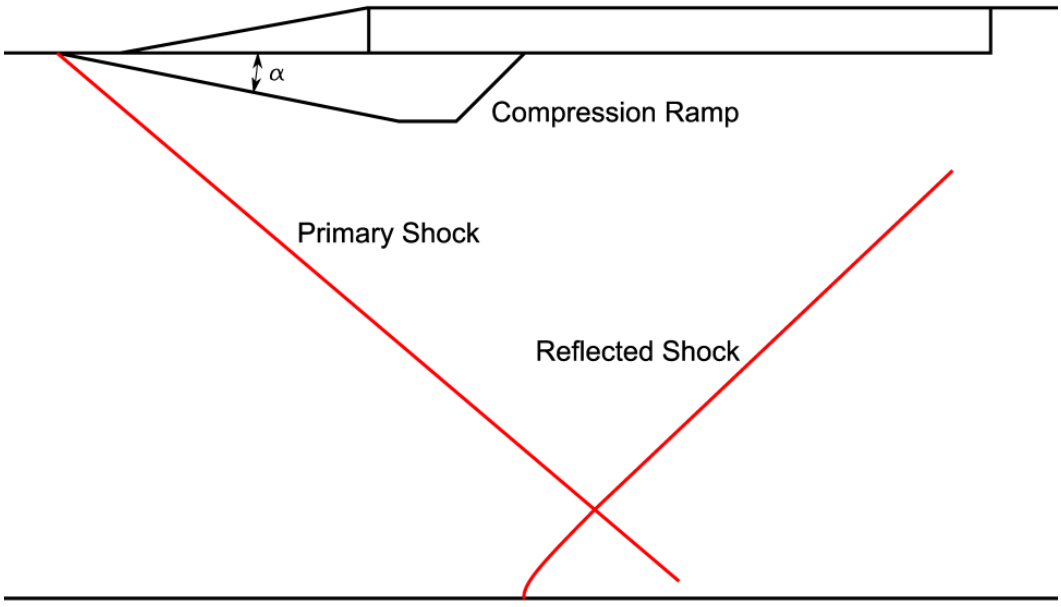

Figure 12: Trimmed Compression Ramp (Note the flat peak)

The new shock system with the trimmed ramp is shown in Figure 13. The primary shock, reflected shock and upstream extraneous shocks remained the same. However, the expansion fan was affected by the modification. There are now two expansions fans with the first developing where the ramp flattens and the second at the trailing edge of the ramp. The first expansion fan of the trimmed compression ramp did impinge on the boundary further upstream of the untrimmed ramp expansion fan: compare Figure 11 and Figure 13. However, its impingement was still downstream of the interaction which was desired. Therefore, trimming the compression

ramp did not affect the SWBLI but it did provide more area to prevent the tunnel from unstarting.

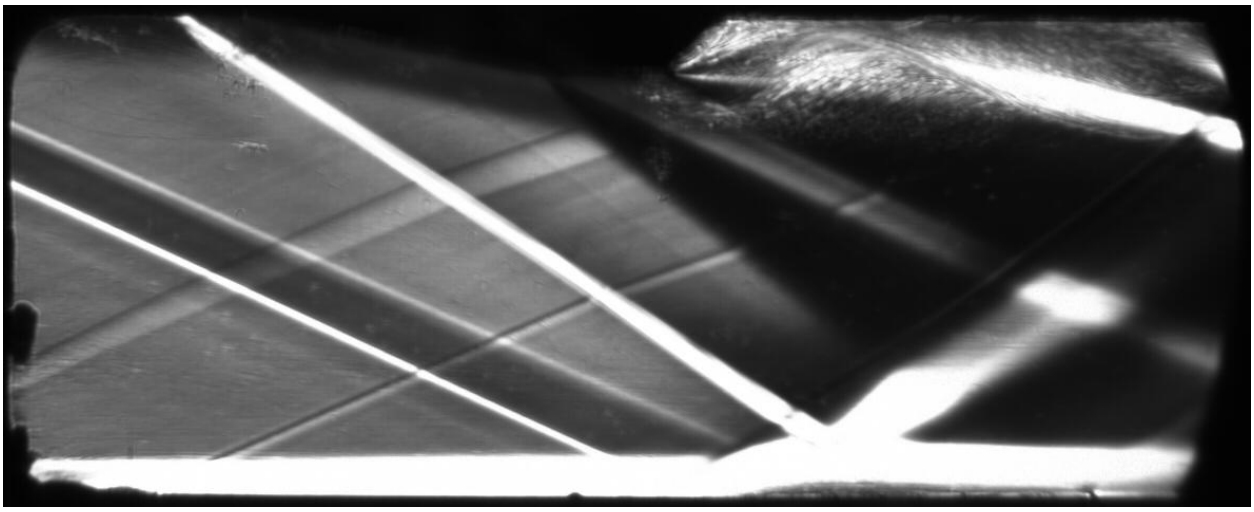

Figure 13: Schlieren Image of Flow with Trimmed Compression Ramp

As discussed earlier, schlieren imaging provided a method to measure the interaction length. The interaction length was calculated by extrapolating the incident and reflected shocks to the floor. The interaction length was measured to be 39 mm, and it was used to normalize the streamwise coordinate and the actuator location. The definition for the interaction length is shown in Figure 14.

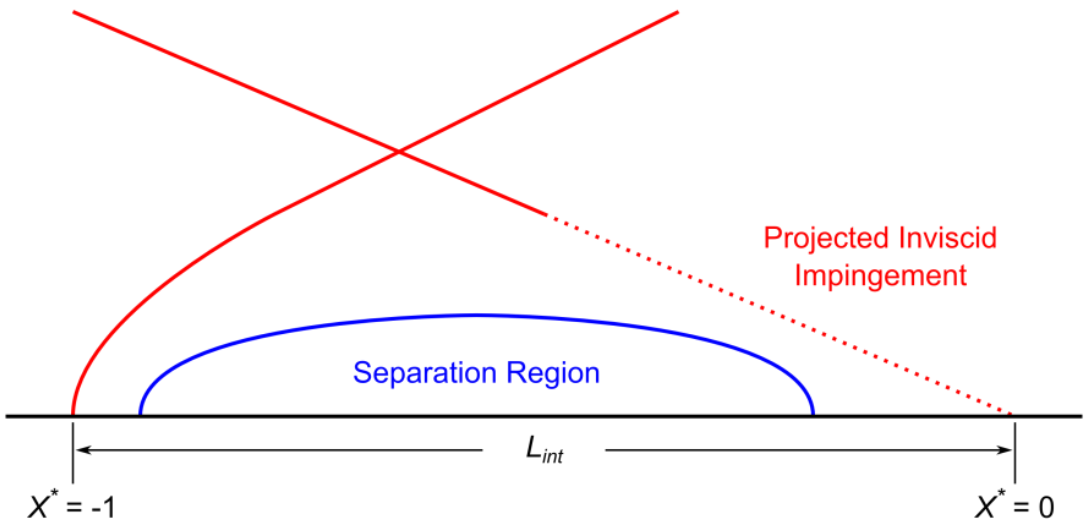

Figure 14: Schematic of Interaction and Separation Region with Definition of Interaction Length and Streamwise Normalization Distances

The projection of the incident shock to the tunnel floor determined the impingement point location. This point was the datum for defining the actuator location and the streamwise distances. The streamwise locations were normalized by the interaction length and are noted as X*. Since the impingement point was the datum, it was denoted by X* = 0. Downstream measurements were positive values and upstream values are negative. Therefore, the reflected shock location was one interaction length upstream denoted by X* = -1. This definition of normalized streamwise length was used in further results.

The schlieren images shown previously were recorded with a horizontal knife edge, but later, the measurement system was altered to use a vertical knife edge. The movement to a vertical knife edge was motivated by the desire to see the reflected shock more clearly. A vertical knife edge accomplished this by providing images of density gradients in the horizontal direction. Across the shock waves, the density goes through a sharp rise; therefore, the primary

and reflected shock appeared similarly as a dark line. Expansion waves appeared as lighter shades because they provide a gradient where the density decreases. This imaging technique provided a clearer view of the shock system but it did not show the boundary layer or separation very clearly. Figure 15 provides an image of the shock system using a vertical knife edge, with the reflected shock being clearly seen.

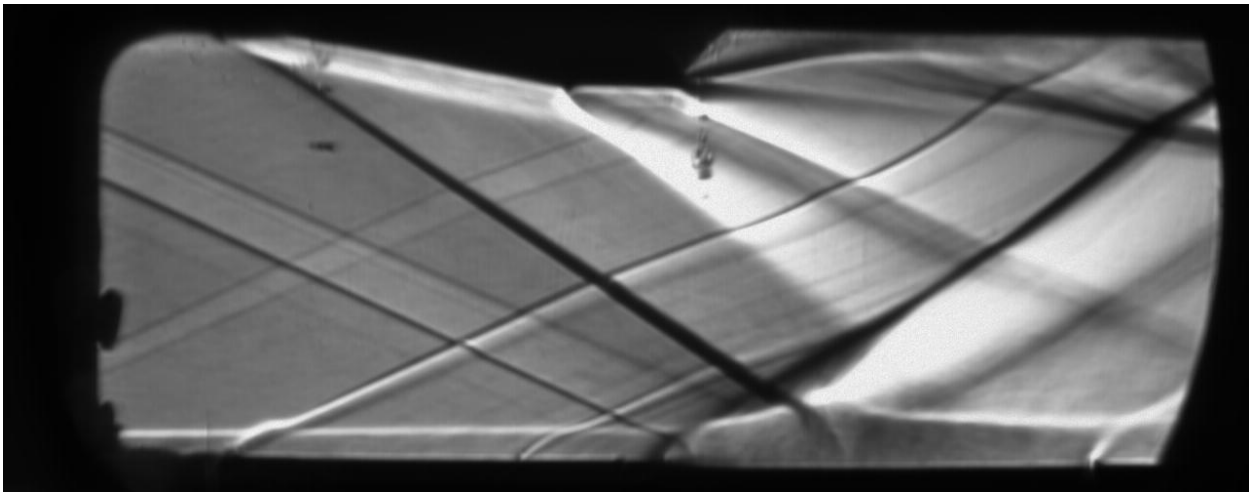

Figure 15: Schlieren Image Using a Vertical Knife Edge

In summary, the schlieren images showed that the shock system was as expected. The primary shock was formed at the foot of the compression ramp and impinged on the boundary layer on the floor. There were not any extraneous shocks that had a noticeable effect on the flow and the expansion fans impinged on the boundary layer downstream of the reattachment point.

5.3 Surface Oil Flow Visualization

Surface oil flow visualization was also used to characterize the baseline flow. The motivation was to observe the separation and determine the three dimensionality of the interaction. The mixture of SAE 85W-140 gear oil, oil pigment, and oleic acid provided the

necessary viscosity to be smeared by the flow shear forces without being blown downstream. This technique both confirmed the presence of and provided a visual image of the flow separation. Figure 16 provides a deskewed image of the test section floor while the tunnel was running with the flow moving from left to right.

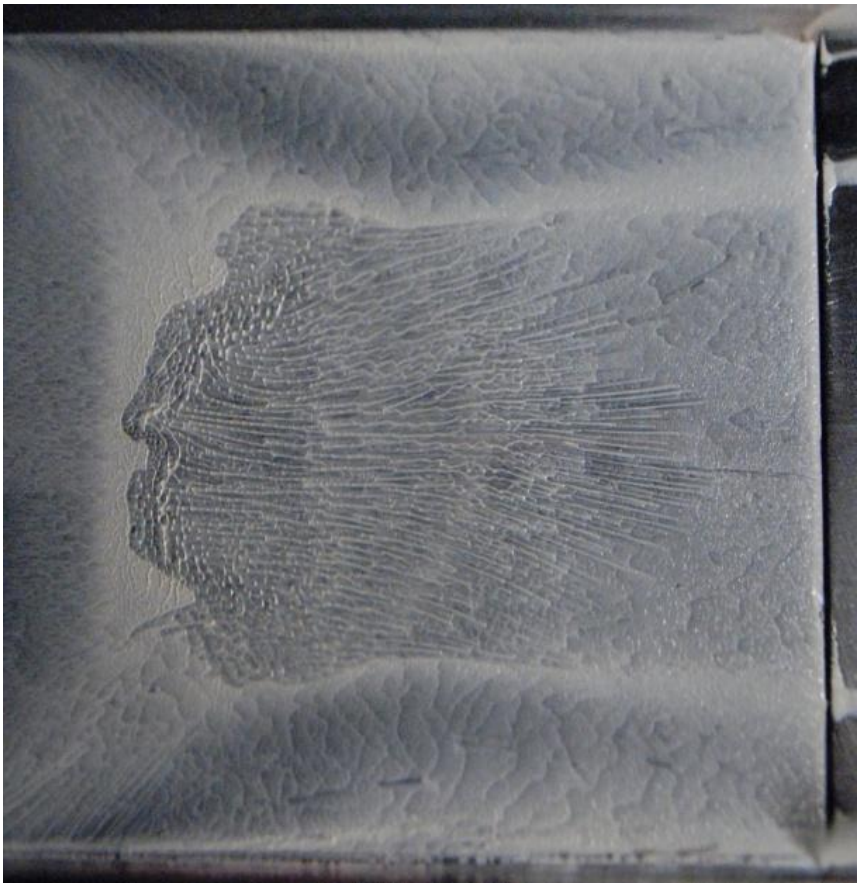

Figure 16: Image Taken while the Tunnel was Running (Flow from Left to Right)

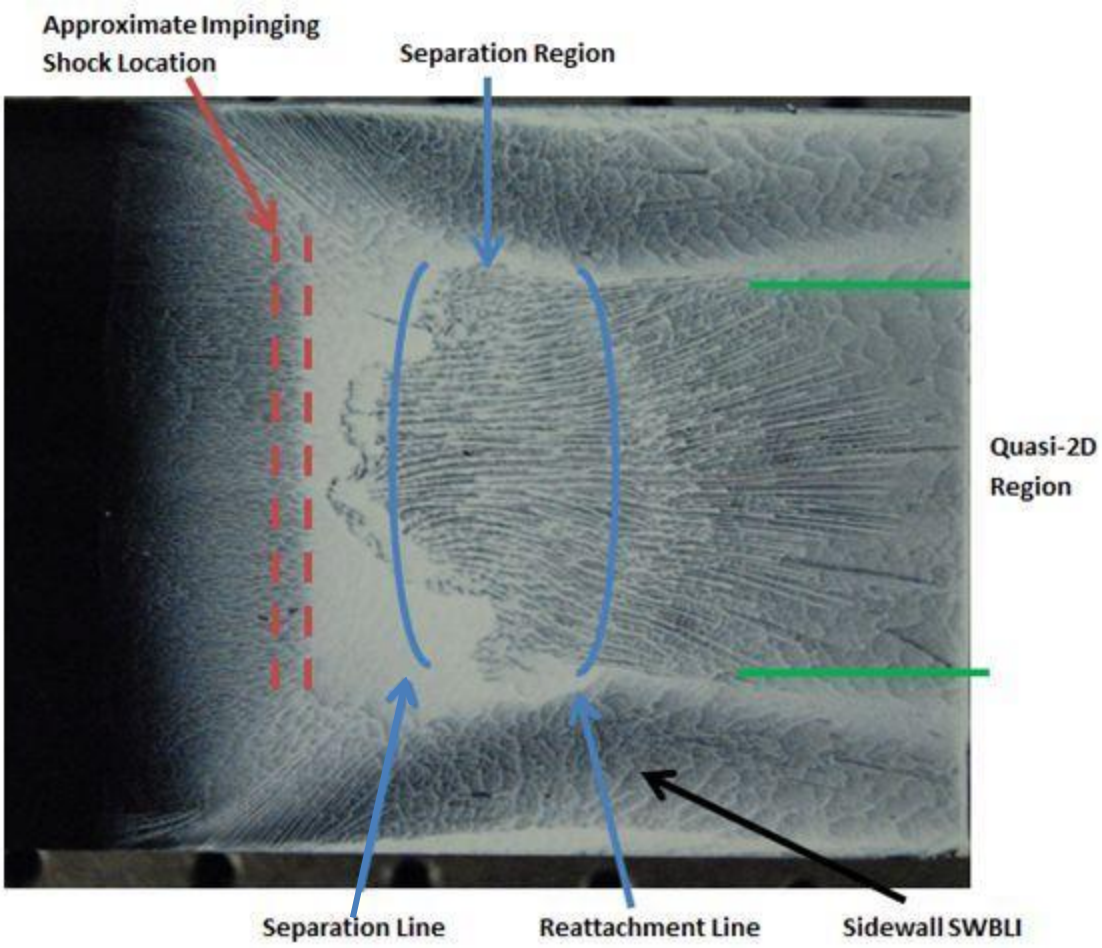

Figure 17: Overhead Image Taken after the Tunnel was Stopped (Flow from Left to Right)

Figure 17 is an overhead image taken after the tunnel was shut down. Even though the tunnel was shut down quickly the mixture did begin to push back into the separation region, but these effects were minimal. The annotated figure identifies structures of the interaction. The impingement location was the point near the reflected shock where the separation began. The build-up of oil in this location was a result of the separation because the flow was no longer moving downstream.

The separation region was also visible as the streaking of the oil was moving upstream rather than downstream. The approximate separation and the reattachment line were indicated

with their curvature being a result of the three dimensionality of the flow. The reattachment line was distinguishable because it was where the flow began to move downstream again. The separation length was measured to compare with the interaction length. The max length of separation was 34.6 mm with a mean separation of 30.79 mm. Due to the possible effect the oil may have had on the separation size, the interaction length was used for normalization throughout this work.

The dimensionality of the flow corresponded to the effects of the side walls. The shock waves interacted with the boundary layer of the side walls and caused the flow to separate there as well. This is a phenomenon of the wind tunnel facility and does not accurately simulate a SWBLI in axisymmetric mixed compression inlets. In this style of facility, the side wall effects are unavoidable so measurements were taken in the two dimensional region with the three dimensionality of the flow documented. The separation of the flow was found to have a two dimensional extent spanning 46% of the tunnel width.

5.4 PIV Imaging

Particle image velocimetry was taken of a streamwise plane on the tunnel centerline in order to quantitatively observe the boundary layer, the shock structure, and the fluid velocities. In regard to the boundary layer, PIV was used to measure the thickness with the measured thickness being 5.28 mm. This component was used to normalize the vertical component in the PIV images. Two PIV images are shown in Figure 18 providing contour maps of the horizontal and vertical velocity components. The vertical coordinate was normalized by the boundary layer thickness, the streamwise component was normalized by the interaction length, and the velocity was normalized by the free stream velocity. The incident and reflected shocks can be seen by the change in velocity of the color gradient. The shocks were more noticeable in the vertical

velocity vector field because the free stream flow had no vertical velocity, but the shock waves altered the flow direction introducing a noticeable vertical component. These images provided shock locations and quantitative verification of the flow velocities. The separation was also shown in the images by the low speed fluid near the floor.

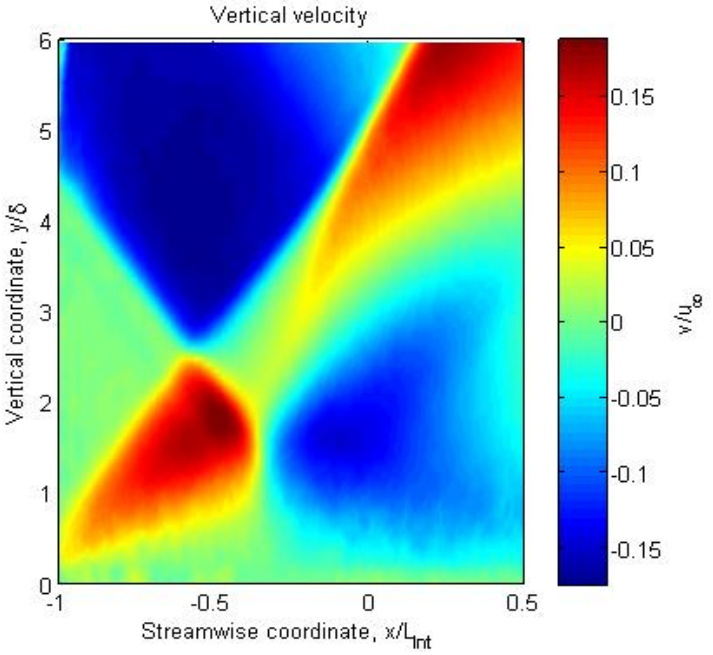

(a)

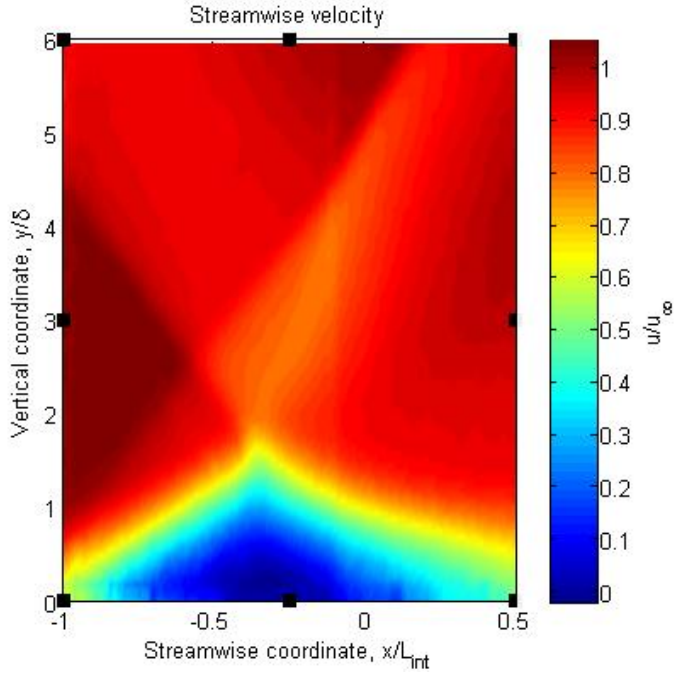

(b)

Figure 18: PIV Images of the Tunnel Centerline (a) Vertical Velocity (b) Streamwise Velocity

A normalized velocity profile for this facility was taken using PIV and is shown in Figure 19. Table 1 also provides a list of the incoming boundary layer data for the facility. The upstream boundary layer conditions are very important in understanding the SWBLI. These parameters provide information on the turbulence which can affect the ability for the flow to separate as well as the separation length. Therefore, it is very important to know these conditions and the state of the upstream boundary layer for characterization of the interaction as well as a better understanding of it.

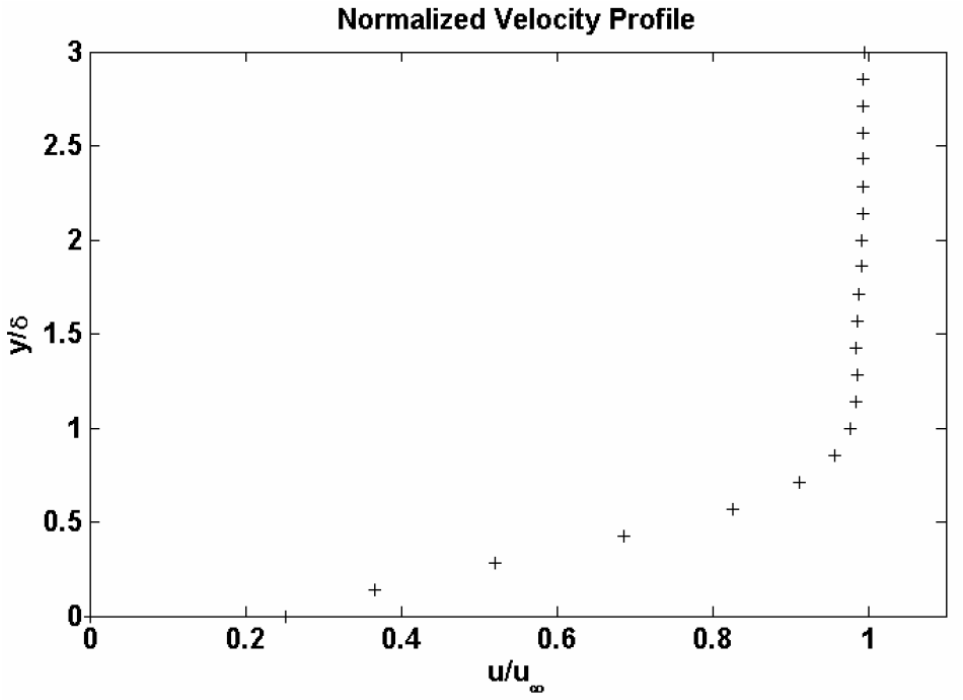

Figure 19: Facility Incoming Boundary Layer Profile (Webb, 2010)

Table 1: Incoming Boundary Layer Data

	Mach	δ (mm)	δ* (mm)	θ (mm)	H	Re_θ
Variable Compression Ramp Facility	2.3	5.28	2.28	.53	4.27	24,800

Furthermore, velocity profiles of the flow were observed to characterize the interaction. The velocity profiles illustrate the separation and shock effect on the velocity. Five profiles were extracted from the velocity maps and there streamwise locations are shown in Figure 20, and their velocity profiles are shown in Figure 21.

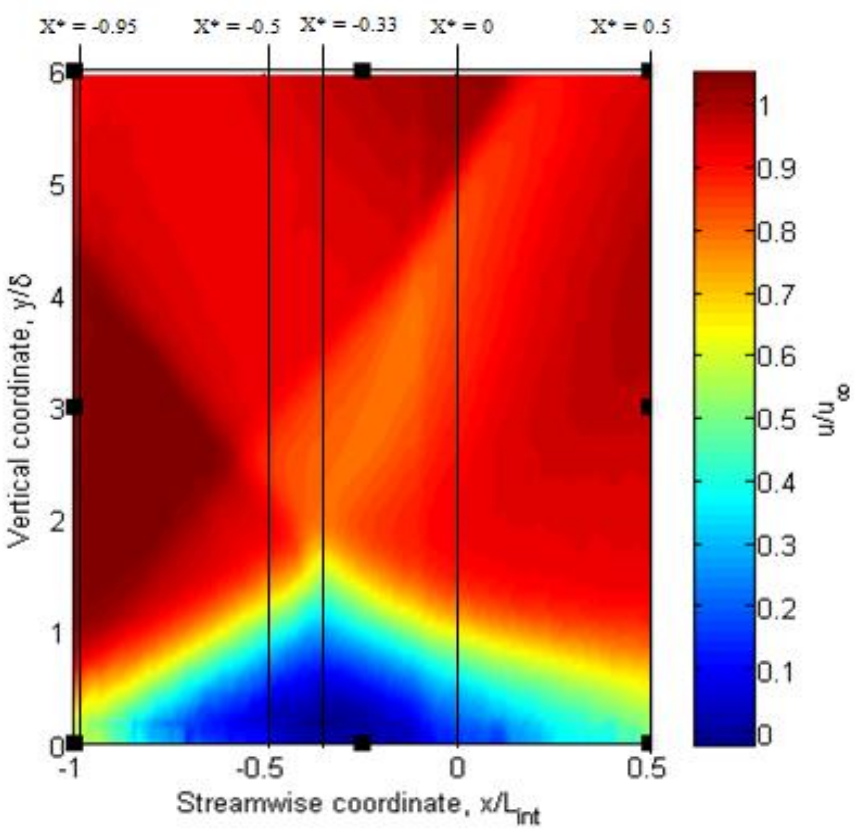

Figure 20: Location of Velocity Profile Planes

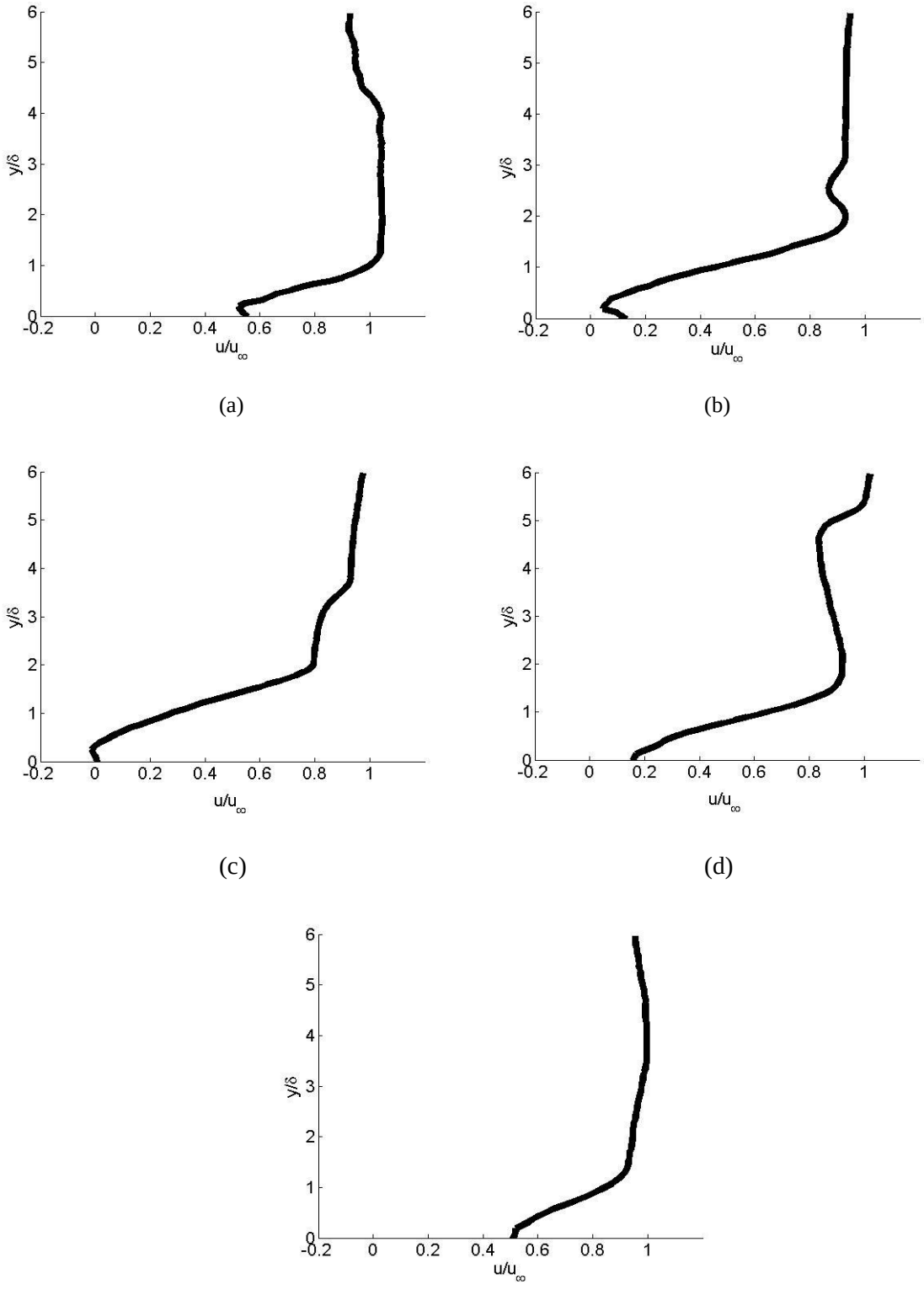

Figure 21: Normalized Velocity Profiles in Planes of different locations. (a) X*=0.-.95 (b) X* = -0.5 (c) X* = -0.33 (d) X*=0 (e) X*=0.5

The normalized velocity at one boundary layer thickness would be at 98% of the free stream velocity because of the definition of boundary layer used in this work. An example of this is shown in Figure 19. However, these profiles were not taken of a healthy boundary layer but include the shocks and separation of the interaction. It is also worth noting that the velocities near the wall were difficult to measure using PIV so although these profiles should have begun at a velocity of zero the profiles did not show this because of inaccurate measurements near the wall.

The profile furthest upstream, X* = -0.95 provided a profile nearest to the incoming boundary layer profile. However, the velocity did not reach free stream velocity until after one boundary thicknesses because of the effects from the leading edge of the separation. As the vertical component continued to increase, the velocity decreased as it encountered the primary shock. The profile showed the shock effect on reducing the flow velocity throughout the measured field. As the observation location moved downstream into the separation the flow velocities were strongly affected, not allowing the profiles to reach the free stream velocity for X* = -0.5 and X* = -0.33. The reduced velocity caused a much lower momentum of the fluid in the separation and a thicker boundary layer.

As the profiles moved further away from the separation, the flow began to recover to near free stream velocities with X* = 0.5 being similar to X* = -0.95 except with a thicker boundary layer. These profiles provided profiles of the interaction effect on fluid flow as it proceeded through the flow separation. The SWBLI hindered the flow velocity strongly especially in the X* = -0.33 case where the velocity did not reach a normalized velocity of .8 until twice the boundary layer thickness. These effects certainly disrupted the flow showing the undesirable effects of the interaction.

5.5 Unsteady Pressure Measurements

Unsteady pressure measurements characterize the unsteady nature of the SWBLI. Dupont et al. (2006) and Touber and Sandham (2009) have found SWBLIs to have a low frequency unsteady nature at frequencies scaled on the interaction length, Strouhal number. Their studies have shown an unsteadiness near the locations of the reflected shock and the reattachment line to have a weighted PSD peak centered at St=0.03 and St=0.5, respectively. Therefore, SWBLIs are expected to have oscillations around St=0.03 near the separation point and St=0.5 near the reattachment point.

Unsteady pressure measurements were taken with the floor shown in Figure 9. The Kulite locations were calculated and normalized based on the interaction length. The results of the measurements are shown in a weighted power spectral density plot shown in Figure 22.

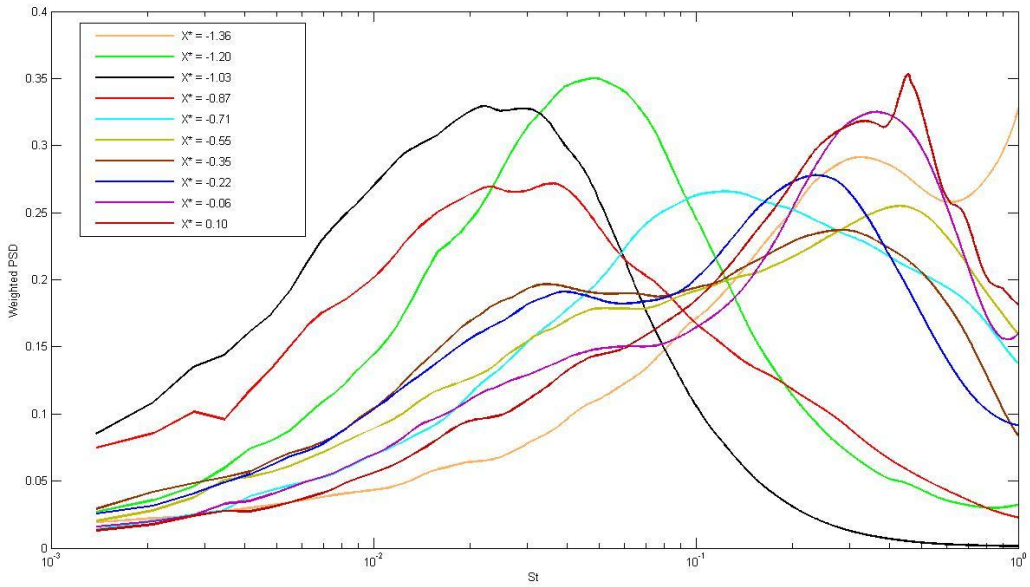

Figure 22: Weighted Power Spectral Density Plots of Wall Pressure Measurements within the SWBLI

The unsteady pressure measurements show that the SWBLI generated in the 10^{o} compression ramp did have the expected unsteady nature. The transducers placed near the reflected shock location, X* = -1.20, -1.03, and -0.87, have all shown a frequency density with a peak around St=0.03 verifying the low frequency unsteadiness associated with the shock foot. Furthermore, the transducers placed near the reattachment region, X* = -0.55, -0.35, -0.22, -0.06, and -0.1, showed peaks around St=0.5 verifying the unsteadiness associated with the reattachment point.

There were two transducers that did not exhibit peaks in these areas. The transducer placed at X* = -1.36 had a magnitude that proceeds upward to a peak beyond St=1. This transducer was upstream of the interaction so it was most likely detecting the high frequency content of the turbulent upstream boundary layer. The other transducer placed at X* = -0.71 had a peak at St=0.1. This peak was in the middle of St=0.03 and St=0.5 so this was believed to be a transducer measuring the transition between the two low frequency oscillations. This transducer splits these peaks, and interestingly it was also at the location that was between the two groups of transducers that correlated to the distinct peaks.

The unsteady pressure measurements have shown that the unsteady nature of our interaction is in agreement with SWBLIs. This also agrees with Dupont et al. (2006) and the unsteadiness that they have found in similar flow of Mach 2.3 that uses an incident oblique shock to generate the SWBLI.

Chapter 6: Summary and Future Work

This study examined the flow of a supersonic wind tunnel with a new shock generator. A 10^{o} compression ramp was used to generate the SWBLI on the tunnel floor. This new ramp reproduced the interaction used in previous research to generate the SWBLI. Characterization of the tunnel was performed to verify its interaction and its baseline flow before forcing experiments were conducted.

The flow was characterized qualitatively through schlieren imaging and surface oil flow visualization. Schlieren imaging provided a view of the shocks and the separation to verify that the tunnel generated the expected interaction. The tunnel did produce the primary shock, reflected shock, separation, and expansion waves as expected. Surface oil flow visualization provided an observation of the flow separation. The flow was separated and the interaction was three dimensional due to the interactions on the side walls. The two dimensional region was found to span 46% of the tunnel width.

The flow and interaction was characterized quantitatively through particle image velocimetry and unsteady pressure measurements. The velocity fields provided quantitative confirmation of the schlieren images. Velocity profiles of this flow showed the detrimental decrease in flow velocity and boundary layer health due to the increase in the boundary layer thickness from separation. The unsteady pressure measurements verified the low frequency unsteady behavior of the shock foot and reattachment line is in agreement with the measurements of Dupont et al. (2006) and Touber and Sandham (2009).

This tunnel has been characterized sufficiently to demonstrate that it does model a typical SWBLI. Further characterization can be performed to measure the unsteadiness associated with the incident shock formed at the compression ramp and to calculate the total pressure recovery

through static pressure measurements. This supersonic wind tunnel facility provides a shock wave/boundary layer interaction that is a suitable environment in which to test the LAFPAs. Furthermore, it provides an area to research the interaction and the mechanisms associated with its unsteadiness. Further pursuit of research of this interaction may provide information regarding the dynamics of the SWBLI to the flow control community.

Chapter 7: References

Anderson, B. H., J. Tinapple, et al. (2006). Optimal Control of Shock Wave Turbulent Boundary Layer Interactions Using Micro-Array Actuation. AIAA 3rd Flow Control Conference. San Francisco, California, June 5-8. AIAA Paper: 1-14.

Babinsky, H., Y. Li, et al. (2009). "Microramp Control of Supersonic Oblique Shock-Wave/Boundary-Layer Interactions." AIAA Journal 47(3): 668-675.

Caraballo, E., N. Webb, et al. (2009). Supersonic Inlet Flow Control Using Plasma Actuators. AIAA 47th Aerospace Sciences Meeting and Exhibit. AIAA Paper: 14.

Clifford, C. (2010). Design and Characterization of a Supersonic Wind Tunnel for the Study of Shock Wave Boundary Layer Interactions. Mechanical Engineering. Columbus, The Ohio State University. Bachelor of Science: 58.

Dolling, D. S. (2001). "Fifty Years of Shock-Wave/Boundary-Layer Interaction Research: What Next?" AIAA Journal 39(8): 1517-1531.

Dupont, P., C. Haddad, et al. (2006). "Space and time organization in a shock-induced separated boundary layer." Journal of Fluid Mechanics 559: 255–277.

Kalra, C. S., S. H. Zaidi, et al. (2011). "Shockwave-Turbulent Boundary Layer Interaction Control Using Magnetically Driven Surface Discharges." Experiments in Fluids 50: 547-559.

Leonov, S. and D. Yarantsev (2008). "Near-Surface Electrical Discharge in Supersonic Airflow: Properties and Flow Control." Journal of Propulsion and Power 24(6): 1168-1181.

Ogawa, H. and H. Babinsky (2008). Shock/Boundary-Layer Interaction Control Using Three-dimensional Bumps in Supersonic Engine Inlets. AIAA 46th Aerospace Sciences Meeting and Exhibit. Reno, Nevada, Jan. 7-10. AIAA Paper: 1-15.

Piponniau, S., J. Dussauge, et al. (2009). "A Simple Model for Low-Frequency Unsteadiness in Shock-Induced Separation." Journal of Fluid Mechanics 629: 87-108.

Samimy, M., I. Adamovich, et al. (2004). "Development and characterization of plasma actuators for high-speed jet control." Experiments in Fluids 37(4): 577-588.

Samimy, M., J.-H. Kim, et al. (2007). "Active Control of a Mach 0.9 Jet for Noise Mitigation Using Plasma Actuators." AIAA Journal 45(4): 890-901.

Samimy, M., J.-H. Kim, et al. (2007). "Active Control of High-Speed and High-Reynolds-Number Jets Using Plasma Actuators." Journal of Fluid Mechanics 578(1): 305-330.

Samimy, M., J.-H. Kim, et al. (2010). "Acoustic and flow fields of an excited high Reynolds number axisymmetric supersonic jet." Journal of Fluid Mechanics 656: 507-529.

Syberg, J. and J. L. Koncsek (1976). "Experimental Evaluation of an Analytically Derived Bleed System for a Supersonic Inlet." Journal of Aircraft 13(10): 792-797.

Touber, E. and N. D. Sandham (2009). "Large-Eddy Simulation of Low-Frequency Unsteadiness in a Turbulent Shock-Induced Separation Bubble." Springer: 79-107.

Webb, N. (2010). Control of Supersonic Mixed-Compression Inlets Using Localized Arc Filament Plasma Actuators. Mechanical Engineering. Columbus, The Ohio State University. Master of Science: 90.